

A Hexagonal Planar Transition Metal Complex

Martí Garçon,^[a] Clare Bakewell,^[a] George A. Sackman,^[b,c] Andrew J. P. White,^[a]
Richard I. Cooper,^[b] Alison J. Edwards,^[c] Mark R. Crimmin^{[a]*}

^[a]Department of Chemistry, Molecular Sciences Research Hub Imperial College London,
White City, London, W12 0BZ, UK.

^[b]Chemical Crystallography, Chemistry Research Laboratory, 12 Mansfield Road, Oxford,
OX1 3TA, UK.

^[c] Australian Centre for Neutron Scattering, Australian Nuclear Science and Technology
Organisation.

*Corresponding author. E-mail: m.crimmin@imperial.ac.uk

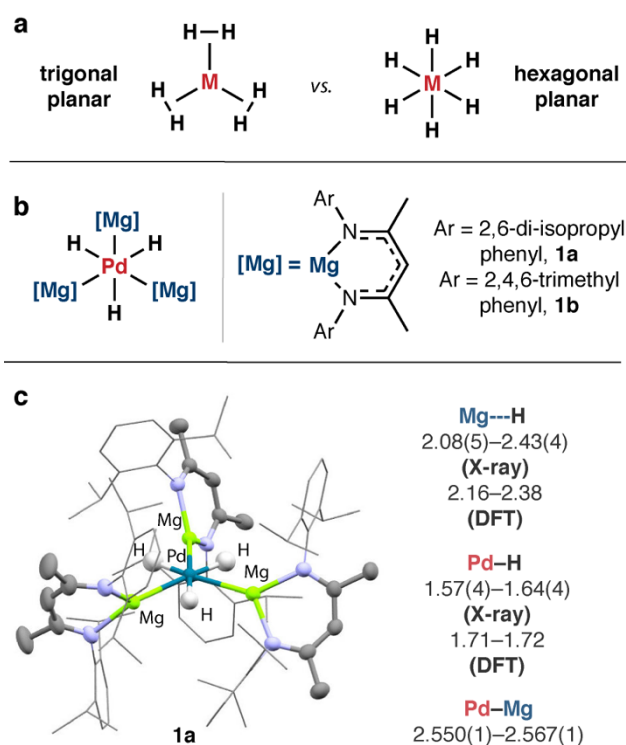
Transition metal complexes are widely applied in the physical and biological sciences. They play pivotal roles in aspects of catalysis, synthesis, materials science, photophysics and bioinorganic chemistry. Our understanding of transition metal complexes originates from Alfred Werner's realisation that their three-dimensional shape influences their properties and reactivity.¹ The intrinsic link between shape and electronic structure is now firmly underpinned by molecular orbital theory.²⁻⁵ Despite over a century of advances in this field, transition metal complexes remain limited to a handful of well understood geometries. Archetypal geometries for six-coordinate transition metals are octahedral and trigonal prismatic. Although deviations from ideal bond angles and lengths are common,⁶ alternative parent geometries are staggeringly rare.⁷ Hexagonal planar transition metals are restricted to those found in condensed metallic phases,⁸ the hexagonal pores of coordination polymers,⁹ or clusters containing more than one transition metal in close proximity.^{10,11} Although $[\text{Ni}(\text{P}^t\text{Bu})_6]$ could be assigned as a hexagonal planar complex,^{12,13} a molecular orbital analysis ultimately led to the conclusion that it is best described as a 16-electron complex with a trigonal planar geometry.¹⁴ Here we report the isolation and structural characterisation of the first simple coordination complex in which six ligands form bonds with a central transition metal in a hexagonal planar arrangement. The discovery has the potential to open up new design principles and new ways of thinking about transition metal complexes which could impact multiple fields of science.

A robust assignment of the coordination geometry of transition metal complexes requires an understanding of both the position of the ligands and the nature of the chemical bonding. For example, consider six hydrogen atoms around a central metal in a planar arrangement.¹⁵ Two extreme cases can be defined. Either a trigonal planar geometry in which the electrons reside within three H–H bonds or a hexagonal planar geometry in which all the H–H bonds are broken and six new M–H interactions are formed. The two representations are limits of a continuum of bonding scenarios (Fig. 1a). While both models are theoretical, the hexagonal planar geometry is expected to be entirely unreasonable due to the combination of the high formal oxidation state of the transition metal and the strongly σ -donating hydride ligands in the equatorial plane. We hypothesised that a plausible approach to obtain the hexagonal planar geometry would be to combine an alternating array of σ -donating (L_σ) and σ -accepting ligands (L_{σ^*}) around the metal. This ligand topology is expected to reduce the formal oxidation state of the metal¹⁶⁻¹⁸ and favour the equatorial arrangement due to weak residual $L_{\sigma} \cdots L_{\sigma^*}$ interactions. In previous work, we¹⁹ and others²⁰⁻²² have shown that magnesium, zinc and gallium hydrides can coordinate to transition metals. In certain cases, the metal–hydride bond can break, leading to the formation of pairs of σ -donating and σ -accepting ligands.

The hexagonal planar complexes **1a** and **1b** were prepared by combining a suitable palladium precursor with a β -diketiminato ligand stabilised magnesium reagent (Fig. 1b, see Methods for synthetic details). Single-crystal X-ray diffraction studies were conducted (Fig. 1c). The data were of sufficient quality that the hydride ligands could be located from the difference density map and their positions confirmed by Density Functional Theory (DFT) calculations.²³ **1a** and **1b** both possess a hexagonal planar geometry at palladium with six ligands forming an equatorial plane in a near perfect hexagonal arrangement. The Mg–Pd–H bond angles range between 54(2) and 67(2) ° with an average value of 60(2) °. The sum of the angles around Pd is 360 ° for both **1a** and **1b**. The largest deviation of the ligands away from the hexagonal plane is $\sim 10^\circ$. Crystallographically characterised Pd–Mg bonds are without precedent. Those in **1a** range from 2.550(1) to 2.567(1) Å while those in **1b** are shorter at 2.485(1) to 2.497(1) Å, both are well within the sum of the single-bond covalent radii (Pauling,²⁴ 2.64 Å; Pyykkö,²⁵ 2.59 Å). The Pd–H bond lengths of **1a** and **1b** are short (1.57(4) to 1.76(4) Å), while the Mg–H bond lengths (2.08(5) to 2.43(4) Å) are beyond the bonding limit of ~ 2.0 Å established in β -diketiminato stabilised magnesium hydride complexes.²⁶ The closest Pd–H–C contacts in

1a are $>2.7 \text{ \AA}$ ($>3.6 \text{ \AA}$ to carbon) and rule out agostic interactions in the axial positions.²⁷ No such contacts are observed in the structure of **1b**.

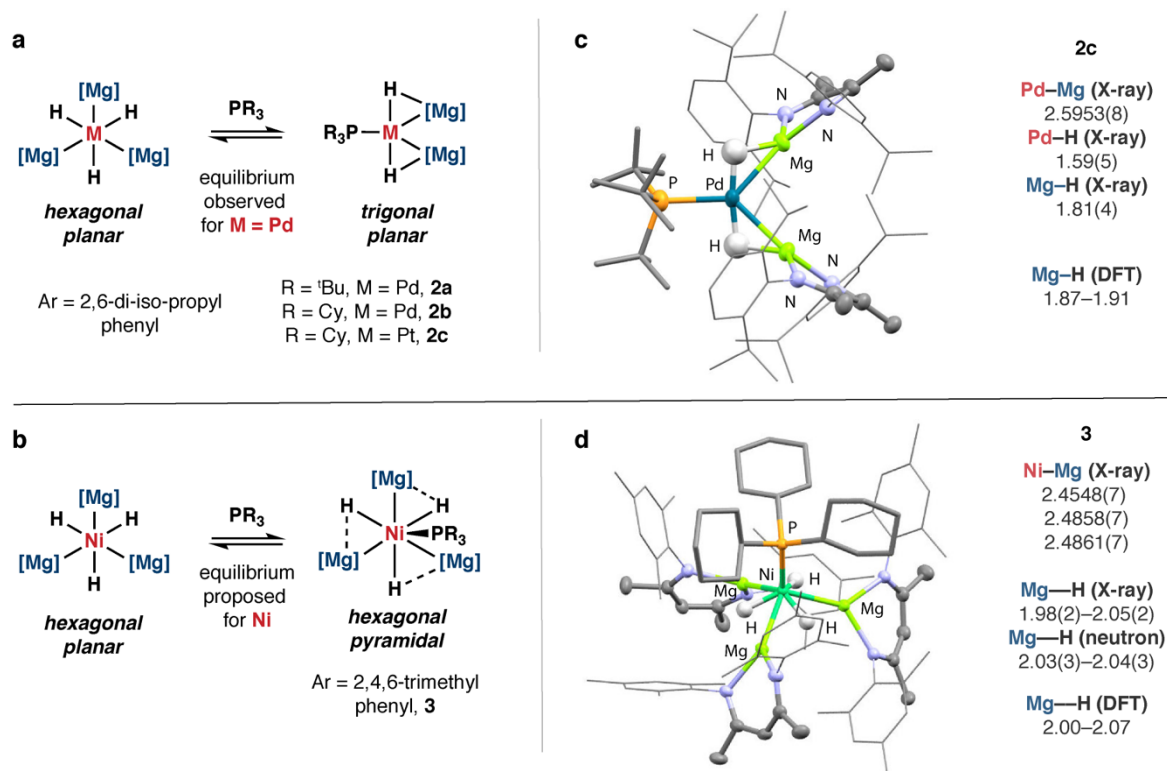
Fig. 1



In further synthetic experiments, the transition metal precursor was varied allowing isolation of **2a–c** and **3** (Fig. 2, see Methods for synthetic details). This remarkable series of complexes provides points of comparison for interrogating the aforementioned hexagonal planar geometry. For example, **2a** contains a distorted trigonal planar geometry. The palladium phosphine dihydride moiety of this complex is T-shaped with a H–Pd–H angle of $172(3)^\circ$ and P–Pd–H angle of $94(1)^\circ$. The Pd–Mg bond lengths in **2a** are approximately 0.05 \AA longer than for **1a**, while the Mg–H distance in **2a** is $0.3\text{--}0.6 \text{ \AA}$ shorter than the Mg---H separations in the hexagonal planar geometry and lie within the normal values expected for a bridging magnesium hydride. A similar structural motif has been observed in a cationic rhodium complex²¹ and is found in the platinum analogue **2c**. In contrast, **3** contains an approximate hexagonal pyramidal geometry that is related to the hexagonal planar form through association of an axial phosphine ligand. The Ni–Mg bond distances of **3** range from $2.455(1)$ to $2.486(1) \text{ \AA}$ and are similar to the sum of the single-bond covalent radii (Pauling,²⁴ 2.51 \AA ; Pyykkö,²⁵ 2.49 \AA). For comparison the Ni---Mg distances in the recently reported $\{\text{Ni}_5\text{Mg}\}$ cluster are longer and range from $2.562(10)$ to $2.947(13) \text{ \AA}$.²⁸ The hydride positions in **3** have

been unambiguously confirmed by a neutron diffraction study. The Mg—H distances of **3** (X-ray: 1.98(2)–2.05(2) Å, neutron: 2.03(3)–2.04(3) Å) are, at their longest, still 0.1–0.3 Å smaller than those observed in the hexagonal planar geometry.

Fig. 2

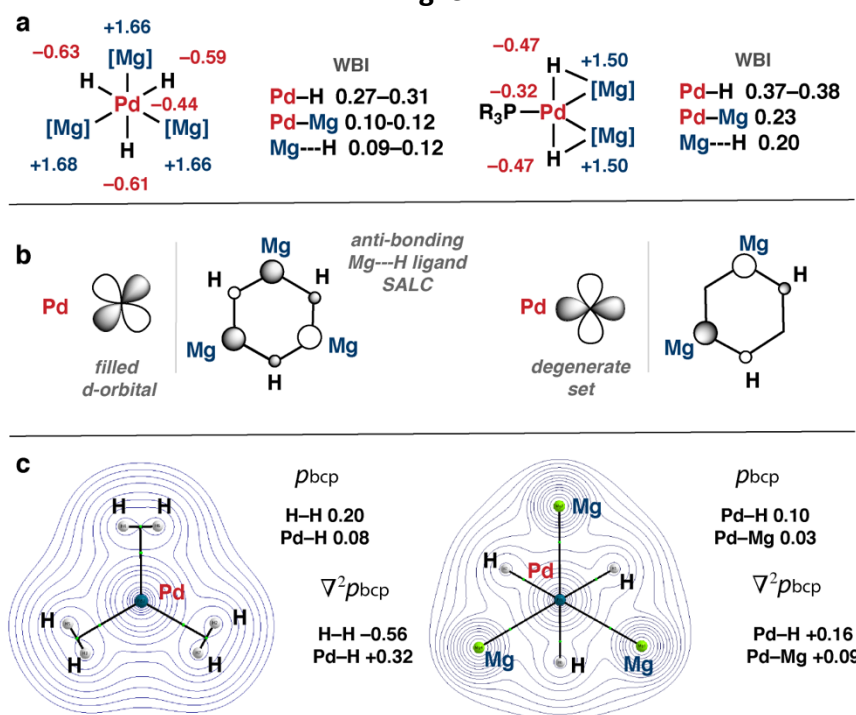


The structures observed in the solid-state persist in solution as evidenced by multinuclear NMR spectroscopy. In THF-*d*₈ solution at 273 K, **3** demonstrates diagnostic resonances in the ¹H and ³¹P{¹H} NMR spectra at δ –7.27 and 53.6 ppm respectively. In C₆D₆, at 298 K **1a** shows a single hydride resonance at δ –1.43 ppm, while **2b** is characterised by ¹H and ³¹P NMR resonances at δ –2.98 and 37.1 ppm respectively. At 283 K, the broad hydride peak of **2b** resolves into a doublet ²J_{P–H} = 9.8 Hz. The coupling constant lies within the 0–20 Hz range established for square-planar complexes bearing a *cis* relation of phosphine and hydride ligands.²⁹ The platinum analogue **2c** displays a similar coupling ²J_{P–H} = 8 Hz, alongside ¹J_{Pt–H} = 833 Hz and ¹J_{Pt–P} = 1594 Hz. For comparison, *trans*-[Pt(H)₂(PCy₃)₂] shows couplings of ²J_{P–H} = 18.8 Hz and ¹J_{Pt–H} = 790 Hz.³⁰ The NMR data are consistent with the *trans*-influence of the hydride ligands in **2b** and **2c** being similar to those found in related square-planar complexes. Variable temperature NMR experiments and titrations show that ligand exchange in this

series of complexes is facile: **2b** exists in equilibrium with both **1a** and $[\text{Pd}(\text{PCy}_3)_2]$, while phosphine dissociation was observed from **3**.

To better understand the hexagonal planar geometry, a series of calculations were undertaken. DFT calculations show that the Pd–Mg interactions of **1a** and **2b** are predominantly ionic in nature. The Mg atoms bear a significant positive charge, while negative charge is localised primarily on the hydride ligands, then on the Pd centre. Evaluation of the Wiberg Bond Indices (WBI) allows an assessment of the size of the covalent contribution to the bonds. The WBIs of the Pd–Mg bonds increase **2b** > **1a** while those of the Mg---H interactions decrease **1a** < **2b** (Fig. 3a). Quantum Theory of Atoms In Molecules (QTAIM) calculations revealed a similar bonding picture. While curved bond critical paths and associated bond critical points were found between the Mg and H atoms in **2b**, these features are all but absent in **1a**. Furthermore, **1a** displays defined bond critical points between the Pd and Mg atoms which are non-existent for **2b** (*supplementary information, Fig. S21*). In combination, these data allow the metal–ligand and ligand---ligand interactions in the hexagonal planar complex to be quantified with some reliability. The calculations show that **1a** has the weakest Mg---H interactions of the series.

Fig. 3



Further insight into the bonding in **1a** can be obtained by considering two simple models. The extreme trigonal planar and hexagonal planar geometries are conveniently described by the 16-electron complexes $[\text{Pd}(\eta^2\text{-H}_2)_3]$ and $[\text{Pd}(\text{H})_3(\text{Mg})_3]^{3+}$. Both can be assigned the D_{3h} point group and described by molecular orbital diagrams (*supplementary information, Fig. S26-27*). Inspection of the Kohn-Sham orbitals for the models provides a qualitative description of the bonding. The key interactions which give rise to the hexagonal planar geometry of $[\text{Pd}(\text{H})_3(\text{Mg})_3]^{3+}$ are a doubly degenerate set of multi-centre two-electron bonds. These can be considered as donor-acceptor interactions between the filled $4d_{xy}$ and $4d_{x^2-y^2}$ orbitals and the corresponding empty ligand SALCs (Symmetry Adapted Linear Combinations) formed from the σ -acceptor ligands (Fig. 3b). The important molecular orbitals of $[\text{Pd}(\eta^2\text{-H}_2)_3]$ are dominated by H-H bonding interactions constructed from the H 1s orbitals. QTAIM calculations returned a near identical breakdown of the electronic structure (Fig. 3c). For $[\text{Pd}(\eta^2\text{-H}_2)_3]$, bond critical paths are found between pairs of H atoms in the ligand sphere. The charge density (ρ_{bcp}) values show that the H-H interactions are more significant than the Pd-H interactions, and the Laplacian of the charge density ($\nabla^2 \rho_{bcp}$) shows charge build up between the hydrogen atom pairs consistent with that expected for a H-H bond. For $[\text{Pd}(\text{H})_3(\text{Mg})_3]^{3+}$ bond critical points are not found between the ligands but are present between Pd and Mg and Pd and H, the bond critical paths radiate out in a hexagonal

arrangement from the central metal atom. Scans of Mg---H bond lengths can be used to interrogate the difference between the hexagonal planar and trigonal planar geometry for $[\text{Pd}(\text{H})_3(\text{Mg})_3]^{3+}$. The potential energy surface that connects these two geometries is almost flat, indicating that compression of the Mg---H interactions requires only a small energy (*supplementary information, Fig. S23*). Nevertheless, the hexagonal planar geometry is the global minimum on this surface for a series of computational methods.

In summary, the data we report all substantiate that **1a–b** are best described as having a hexagonal planar geometry with unprecedented Pd–Mg bonds. The valence electrons reside almost entirely in the metal–ligand bonds with only weak residual interactions remaining between the hydride (L_σ) and magnesium (L_{σ^*}) ligands. Minor perturbations of the structure to either include an axial phosphine ligand, to form **3**, or exchange an equatorial ligand, to form trigonal planar **2a–c**, leads to a measurable contraction of the Mg---H distances and strengthening of the ligand---ligand interactions.

Acknowledgements

We are grateful to the Royal Society and the ERC (FluoroFix: 677367) for generous funding. Johnson Matthey is gratefully acknowledged for the gift of PdCl_2 . ANSTO is thanked for allocation of neutron beam-time on KOALA to proposal P6932.

References

1. Constable, E. C. & Housecroft, C. E. Coordination chemistry: the scientific legacy of Alfred Werner. *Chem. Soc. Rev.* **42**, 1429–1439 (2013).
2. Hoffmann, R., Beier, B. F., Muetterties, E. L. & Rossi, A. R. Seven-Coordination. A Molecular Orbital Exploration of Structure, Stereochemistry, and Reaction Dynamics. *Inorg. Chem.* **16**, 511–522 (1977).
3. Rossi, A. R. & Hoffmann, R. Transition Metal Pentacoordination. *Inorg. Chem.* **14**, 365–374 (1975).
4. Gray, H. B. & Ballhausen, C. J. A Molecular Orbital Theory for Square Planar Metal Complexes. *J. Am. Chem. Soc.* **85**, 260–265 (1963).
5. Gray, H. B. Molecular Orbital Theory for Transition Metal Complexes. *J. Chem. Ed.* **41**, 2–12 (1964).
6. Alvarez, S. Distortion Pathways of Transition Metal Coordination Polyhedra Induced by Chelating Topology. *Chem. Rev.* **115**, 13447–13483 (2015).
7. García-Monforte, M. A., Baya, M., Falvello, L. R., Martín, A. & Menjón, B. An Organotransition-Metal Complex with Pentagonal-Pyramidal Structure. *Angew. Chem. Int. Ed.* **51**, 8046–8049 (2012).
8. Yang, L.-M. *et al.* Two-Dimensional Cu₂Si Monolayer with Planar Hexacoordinate Copper and Silicon Bonding. *J. Am. Chem. Soc.* **137**, 2757–2762 (2015).
9. Niu, Z., Ma, J.-G., Shi, W. & Cheng, P. Water molecule-driven reversible single-crystal to single-crystal transformation of a multi-metallic coordination polymer with controllable metal ion movement. *Chem. Commun.* **50**, 1839–1842 (2014).
10. Tanabe, M. *et al.* Tetrapalladium Complex with Bridging Germylene Ligands. Structural Change of the Planar Pd₄Ge₃ Core. *J. Am. Chem. Soc.* **133**, 18598–18601 (2011).
11. Yamada, T., Mawatari, A., Tanabe, M., Osakada, K. & Tanase, T. Planar Tetranuclear and Dumbbell-Shaped Octanuclear Palladium Complexes with Bridging Silylene Ligands. *Angew. Chem. Int. Ed.* **48**, 568–571 (2009).
12. Ahlrichs, R., Fenske, D., Oesen, H. & Schneider, U. Synthesis and Structure of [Ni(PtBu)₆] and [Ni₅(PtBu)₆(CO)₅] and Calculations on the Electronic Structure of [Ni(PtBu)₆] and (PR)₆, R = tBu, Me. *Angew. Chem. Int. Ed.* **31**, 323–326 (1992).
13. Hey Hawkins, E., Pink, M., Oesen, H. & Fenske, D. Syntheses and Characterization of [Ni(tBuAs)₆] and [Pd(tBuAs)₆]. *Z. Anorg. Allg. Chem.* **622**, 689–691 (1996).
14. Tang, H., Hoffman, D. M., Albright, T. A., Deng, H. & Hoffmann, R. [Ni(PtBu)₆] and [Ni(SiH₂)₆] Are Isolobal, Related to [In{Mn(CO)₄]₅]²⁻, and Have 16-Electron Counts. *Angew. Chem. Int. Ed.* **32**, 1616–1618 (1993).
15. Kubas, G. J. Dihydrogen complexes as prototypes for the coordination chemistry of saturated molecules. *Proc. Natl. Acad. Sci.* **104**, 6901–6907 (2007).
16. Crabtree, R. H. Chemistry: A New Oxidation State for Pd? *Science* **295**, 288–289 (2002).
17. Chen, W., Shimada, S. & Tanaka, M. Synthesis and Structure of Formally Hexavalent Palladium Complexes. *Science* **295**, 308–310 (2002).
18. Aullón, G., Lledós, A. & Alvarez, S. Hexakis(silyl)palladium(VI) or Palladium(II) with η²-Disilane Ligands? *Angew. Chem. Int. Ed.* **41**, 1956–1959 (2002).
19. Butler, M. J. & Crimmin, M. R. Magnesium, zinc, aluminium and gallium hydride complexes of the transition metals. *Chem. Commun.* **53**, 1348–1365 (2017).
20. Abdalla, J. A. B. *et al.* Coordination and Activation of Al–H and Ga–H Bonds. *Chem. Eur. J.* **20**, 17624–17634 (2014).
21. Abdalla, J. A. B. *et al.* Structural snapshots of concerted double E–H bond activation at a transition metal centre. *Nat. Chem.* **9**, 1256–1262 (2017).
22. Riddlestone, I. M. *et al.* Activation of H₂ Over the Ru–Zn Bond in the Transition Metal-Lewis Acid Heterobimetallic Species [Ru(IPr)₂(CO)ZnEt]⁺ (IPr = 1,3-bis(2,6-diisopropylphenyl)imidazol-2-ylidene). *J. Am. Chem. Soc.* **138**, 11081–11084 (2016).
23. Sharninghausen, L. S. *et al.* The neutron diffraction structure of [Ir₄(IMe)₈H₁₀]²⁺ polyhydride cluster: Testing the computational hydride positional assignments. *J. Organomet. Chem.* **849-850**, 17–21 (2017).
24. Pauling, L. Atomic Radii and Interatomic Distances in Metals. *J. Am. Chem. Soc.* **69**, 542–553 (1947).

25. Pyykkö, P. & Atsumi, M. Molecular Single-Bond Covalent Radii for Elements 1-118. *Chem. Eur. J.* **15**, 186–197 (2009).
26. Mukherjee, D. & Okuda, J. Molecular Magnesium Hydrides. *Angew. Chem. Int. Ed.* **57**, 1458–1473 (2018).
27. Brookhart, M., Green, M. L. H. & Parkin, G. Agostic interactions in transition metal compounds. *Proc. Natl. Acad. Sci.* **104**, 6908–6914 (2007).
28. Shoshani, M. M., Liu, J. & Johnson, S. A. Mechanistic Insight into H/D Exchange by a Pentanuclear Ni–H Cluster and Synthesis and Characterization of Structural Analogues of Potential Intermediates. *Organometallics* **37**, 116–126 (2017).
29. Kudo, K., Hidai, M. & Uchida, Y. Dihydride complexes of platinum(II) and palladium(II). *J. Organomet. Chem.* **56**, 413–418 (1973).
30. Leviston, P. G. & Wallbridge, M. G. H. The preparation of some bulky dihalo-, halohydrido- and dihydro- phosphineplatinum(II) compounds. *J. Organomet. Chem.* **110**, 271–279 (1976).

Fig. 1 | Preparation of hexagonal planar complexes. **a**, theoretical valence isomers of a hypothetical $[MH_6]$ complexes showing two extreme bonding situations, on the left a trigonal planar geometry on the right a hexagonal planar geometry. **b**, A line-drawing of the hexagonal planar complexes **1a-b** described herein along with a definition of the magnesium fragment $[Mg]$. **c**, single-crystal X-ray derived model of **1a** annotated with selected experimental and calculated bond lengths (\AA).

Fig. 2 | Preparation of group 10 hydride complexes bearing magnesium ligands. **a**, line-drawings of the trigonal planar complexes **2a-c** showing their relationship with the hexagonal planar analogues. **b**, a line-drawing of the hexagonal pyramidal complex **3**. **c-d**, single-crystal X-ray derived model of **2b** and **3** annotated with selected experimental and calculated bond lengths (\AA).

Fig. 3 | Analysis of the chemical bonding in the hexagonal planar geometry. **a**, line-drawings of **1a** and **2b** showing the calculated NPA (Natural Population Analysis) charges on the key atoms, these charges show negative charge accumulation on Pd and H and positive charge accumulation on Mg. The drawings are annotated with Wiberg Bond Indices (WBI) that indicate the strength of the covalent interaction. **b**, key bonding interactions in the model complex $[Pd(H)_3(Mg)_3]^{3+}$ that show donor–acceptor interaction between Pd and Mg/H atoms. **c**, molecular graphs from QTAIM calculations on $[Pd(\eta^2-H_2)_3]$ and $[Pd(H)_3(Mg)_3]^{3+}$ ρ_{bcp} refers to the charge density and $\nabla^2\rho_{bcp}$ to the Laplacian of the charge density at the bond critical point.

Extended Data Fig. 1 | Synthesis of group 10 hydride complexes bearing magnesium ligands. **a**, synthetic scheme for preparation of **1a**. **b**, synthetic scheme for preparation of **2a**. **c**, synthetic scheme for preparation of **2b**. **d**, synthetic scheme for preparation of **2c**. **e**, synthetic scheme for preparation of **3**, the hydride ligands are derived from the C–H bonds of the benzene solvent.

Methods

General Procedures: Unless otherwise specified, all manipulations were carried out using standard Schlenk and glovebox techniques, under inert atmosphere (nitrogen or argon). A MBRAUN Labmaster glovebox was employed operating with concentrations of H₂O and O₂ below 0.1 ppm. Anhydrous solvents were obtained from a Grubbs type SPS system and stored over activated 3 Å molecular sieves under inert atmosphere. Preparation of starting materials is detailed in the *supplementary methods*. All other reagents were obtained from commercial suppliers (Sigma-Aldrich, Alfa Aesar, Fluorochem) and used without further purification.

Synthesis of 1a: Method 1. [Pd(Me)₂(κ²-TMEDA)] (40 mg, 0.16 mmol, 1.0 equiv.) and [Mg(μ-H){(ArNCMe)₂CH}]₂ (Ar = 2,6-di-iso-propylphenyl, 189 mg, 0.21 mmol, 1.35 equiv.) were dissolved in toluene (10 mL). The reaction mixture immediately turned black and was stirred at 25 °C overnight. The volatiles were removed *in vacuo* and the residue washed with a small amount of cold hexane (1 mL). The solid was recrystallised from a *ca.* 1:1 toluene:hexane mixture (2 mL) at -35 °C and the crystals washed successively with small amounts of cold *n*-hexane (0.5 mL x 3), to afford the product **1a** as a dark solid (50 mg, 0.035 mmol, 22 %). Reliable isolation of high purity **1a** *via* this method is problematic, so an alternative method was developed. **Method 2.** In a glovebox, [Pd(η⁵-Cp)(η³-cinnamyl)] (100 mg, 0.35 mmol, 1.0 equiv.) and [Al(H)₂{(ArNCMe)₂CH}] (Ar = 2,6-di-iso-propylphenyl, 325 mg, 0.73 mmol, 2.1 equiv.) were dissolved in benzene (5 mL) to form a dark brown solution, which was left to stand without stirring at 25 °C for 72 h. A red solid slowly precipitated. The mother liquor was decanted, the solid swiftly washed with benzene (2 x 2 mL) and dried under vacuum to yield [PdAl(H)₂{(ArNCMe)₂CH}]₂ as red crystals (95 mg, 0.086 mmol, 50 %). [PdAl(H)₂{(ArNCMe)₂CH}]₂ was used in the next step without further purification. [PdAl(H)₂{(ArNCMe)₂CH}]₂ (50 mg, 0.05 mmol, 1 equiv.) and [Mg(μ-H){κ²-(ArNCMe)₂CH}]₂ (Ar = 2,6-di-iso-propylphenyl, 120 mg, 0.135 mmol, 3 equiv.) were suspended in benzene (5 mL) and the mixture was left stirring at 50 °C for 72 h. The suspension turned into a yellow-orange solution. The solvent was removed *in vacuo* and the residue washed with *n*-hexane (3 x 0.5 mL). The pale brown solid was then dissolved in a 1:1 toluene:*n*-hexane mixture (1 mL),

filtered through a glass fibre to remove small amounts of a black solid assumed to be Pd(0). The solution was stored at $-35\text{ }^{\circ}\text{C}$ and the product crystallised as colourless needles. **1a** was isolated as an off-white solid (33 mg, 0.023 mmol, 26%). **$^1\text{H-NMR}$** (400 MHz, C_6D_6 , 298 K) δ (ppm): -1.43 (s, 3H, PdH_3), 0.96 (d, $^3J_{\text{H-H}} = 6.9$ Hz, 36H, CHMe_2), 1.19 (d, $^3J_{\text{H-H}} = 6.7$ Hz, 36H, CHMe_2), 1.53 (s, 18H, Me), 3.13 (sept, $^3J_{\text{H-H}} = 6.8$ Hz, 12H, CHMe_2), 4.85 (s, 3H, $\beta\text{-CH}$), $6.85\text{--}7.40$ (series of overlapping m, 18H, Ar). **T_1 relaxation time** (PdH_3 signal, 298K): 0.83 s. **$^{13}\text{C}\text{-}\{^1\text{H}\}\text{-NMR}$** (100 MHz, C_6H_6) δ (ppm): 23.7 (12x CH_3), 24.2 (6x CH_3), 25.2 (12x CH_3), 27.9 (12xCH), 95.7 (3xCH), 123.4 (12xCH), 124.8 (6xCH), 142.0 (12xC), 145.4 (6xC), 168.7 (6xC). **IR (ATR, cm^{-1})**: 3056, 2959, 2926, 2866, 1618, 1547, 1431, 1405, 1364, 1312, 1252, 1174, 1100, 1021, 757. **Anal. Calc.** ($\text{C}_{87}\text{H}_{126}\text{Mg}_3\text{N}_6\text{Pd}$): C, 72.80; H, 8.85; N, 5.86. Found: C, 72.66; H, 8.97; N, 5.74. **Crystal data for 1a**: $\text{C}_{87}\text{H}_{126}\text{Mg}_3\text{N}_6\text{Pd}\cdot 0.35(\text{C}_6\text{H}_{14})$, $M = 1465.42$, triclinic, $P-1$ (no. 2), $a = 13.2847(5)$, $b = 13.4347(5)$, $c = 24.7995(10)$ Å, $\alpha = 87.949(3)$, $\beta = 86.394(3)$, $\gamma = 76.189(3)^\circ$, $V = 4288.7(3)$ Å³, $Z = 2$, $D_c = 1.135$ g cm^{-3} , $\mu(\text{Cu-K}\alpha) = 2.293$ mm⁻¹, $T = 173$ K, colourless tablets, Agilent Xcalibur PX Ultra A diffractometer; 16321 independent measured reflections ($R_{\text{int}} = 0.0560$), F^2 refinement, $R_1(\text{obs}) = 0.0463$, $wR_2(\text{all}) = 0.1085$, 12341 independent observed absorption-corrected reflections [$|F_o| > 4\sigma(|F_o|)$], $2\theta_{\text{max}} = 147^\circ$], 981 parameters. CCDC 1909687.

Isolation of 1b: In a J. Young's NMR tube, $[\{(\text{MesNCMe})_2\text{CH}\}\text{Mg}]_2$ (Mes = 2,4,6-trimethylphenyl, 30 mg, 0.04 mmol, 1.0 equiv.) was suspended in dry toluene (1 mL) and $[\text{Pd}(\text{PCy}_3)_2]$ (2.8 mg, 4.2×10^{-3} mmol, 0.10 equiv.) was added. The reaction mixture was left for 48 h at $25\text{ }^{\circ}\text{C}$. Over this time period the reaction mixture turned from turbid to a clear yellow solution. The volatiles were then removed *in vacuo* and the crude was redissolved in *n*-hexane (1 mL) and left at $-35\text{ }^{\circ}\text{C}$. After repeated attempts, a few X-ray quality crystals of **1b** were obtained. Attempts to obtain **1b** on a preparative scale failed. Increasing the palladium loading, resulted in regeneration of $[\text{Pd}(\text{PCy}_3)_2]$. **Crystal data for 1b**: $\text{C}_{69}\text{H}_{90}\text{Mg}_3\text{N}_6\text{Pd}$, $M = 1182.79$, monoclinic, $P2_1/c$ (no. 14), $a = 25.9596(3)$, $b = 12.45210(14)$, $c = 21.1354(3)$ Å, $\beta = 100.3614(12)$, $V = 6720.63(14)$ Å³, $Z = 4$, $D_c = 1.169$ g cm^{-3} , $\mu(\text{Cu-K}\alpha) = 2.817$ mm⁻¹, $T = 173$ K, colourless tablets, Agilent Xcalibur PX Ultra A diffractometer; 12913 independent measured reflections ($R_{\text{int}} = 0.0269$), F^2 refinement, $R_1(\text{obs}) = 0.0449$, $wR_2(\text{all}) = 0.1343$, 10387

independent observed absorption-corrected reflections [$|F_o| > 4\sigma(|F_o|)$], $2\theta_{\max} = 148^\circ$], 748 parameters. CCDC 1909688.

Synthesis of 2a: In a glovebox, $[\text{Mg}(\mu\text{-H})\{\text{ArNCMe}_2\text{CH}\}]_2$ (Ar = 2,6-di-iso-propylphenyl, 26 mg, 0.030 mmol, 1.25 eq.) was added to a solution of $[\text{Pd}(\text{Me})_2(\kappa^2\text{-TMEDA})]$ (TMEDA = tetramethylethylamine, 6 mg, 0.024 mmols, 1 eq.) in dry benzene in a J. Young's NMR tube. A solution of P^tBu_3 (5 mg, 0.023 mmol, 0.95 eq.) in benzene was then added dropwise. Formation of **2a** as well as $[\text{Pd}(\text{P}^t\text{Bu}_3)_2]$ was identified by ^{31}P -NMR spectroscopy. The conversion did not increase after 18 h at 25 °C. The solvent was removed *in vacuo*. In the glovebox, the crude was suspended in dry *n*-hexane, the excess starting material was removed by filtration with a PTFE 0.2 μm HPLC filter and the brown clear solution was left at -35°C to afford crystals of **2a** suitable for X-ray diffraction. **^1H -NMR (500 MHz, C_6H_6 , 283 K)** δ (ppm): -4.49 (s, 2H, PdH_2). **^{31}P - $\{^1\text{H}\}$ -NMR (202 MHz, C_6H_6 , 283K)** δ (ppm): 86.6 (broad s). **Crystal data for 2a:** $\text{C}_{70}\text{H}_{111}\text{Mg}_2\text{N}_4\text{PPd}\cdot 2(\text{C}_6\text{H}_{14})$, $M = 1366.95$, monoclinic, $I2/a$ (no. 15), $a = 15.52641(16)$, $b = 20.9811(2)$, $c = 24.8465(3)$ Å, $\beta = 90.7595(9)^\circ$, $V = 8093.32(14)$ Å³, $Z = 4$ (half a molecule per asymmetric unit), $D_c = 1.122$ g cm⁻³, $\mu(\text{Cu-K}\alpha) = 2.494$ mm⁻¹, $T = 173$ K, brown blocks, Agilent Xcalibur PX Ultra A diffractometer; 8015 independent measured reflections ($R_{\text{int}} = 0.0357$), F^2 refinement, $R_1(\text{obs}) = 0.0435$, $wR_2(\text{all}) = 0.1220$, 7154 independent observed absorption-corrected reflections [$|F_o| > 4\sigma(|F_o|)$], $2\theta_{\max} = 148^\circ$], 500 parameters. CCDC 1589324. **Solution stability:** **2a** is unstable in solution and forms an equilibrium mixture of **2a**, $[\text{Pd}(\text{P}^t\text{Bu}_3)_2]$ and $[\text{Mg}(\mu\text{-H})\{\text{ArNCMe}_2\text{CH}\}]_2$.

Synthesis of 2b: Method 1. In a glovebox, $[\text{Mg}(\mu\text{-H})\{\text{ArNCMe}_2\text{CH}\}]_2$ (Ar = 2,6-di-isopropylphenyl, 50 mg, 0.057 mmol, 2.5 eq.) and $[\text{Pd}(\text{PCy}_3)_2]$ (15 mg, 0.022 mmols, 1 eq.) were dissolved in dry benzene (C_6H_6) in a J. Young's NMR tube. The conversion did not increase after 5 h at 25 °C to give a *ca.* 1:6 $[\text{Pd}(\text{PCy}_3)_2]$: **2b** mixture, as evidenced by ^{31}P -NMR spectroscopy. The solvent was removed *in vacuo*. In the glovebox, the crude was suspended in dry *n*-hexane (1 mL), unreacted $[\text{Mg}(\mu\text{-H})\{\text{ArNCMe}_2\text{CH}\}]_2$ was removed by filtration with a PTFE 0.2 μm HPLC filter and the yellow clear solution was left at -35°C to afford crystals of **2b** suitable for X-ray diffraction. **Method 2.** In a glovebox, $[\text{Mg}(\mu\text{-H})\{\text{ArNCMe}_2\text{CH}\}]_2$ (Ar = 2,6-di-isopropylphenyl, 47 mg, 0.053 mmol, 2.25 eq.) was added to a solution of $[\text{Pd}(\text{Me})_2(\kappa^2\text{-$

TMEDA)] (6 mg, 0.024 mmols, 1 eq.) in dry benzene in a J. Young's NMR tube. A solution of PCy₃ (7 mg, 0.024 mmol, 1 eq.) in benzene was then added dropwise. Immediate formation at 25 °C of **2b** as well as [Pd(PCy₃)₂] was identified by ³¹P-NMR spectroscopy. ¹H-NMR (500 MHz, C₆H₆, 298 K) δ (ppm): -2.98 (s, 2H, PdH₂). Partial data only. ¹H-NMR (400 MHz, C₇D₈, 233 K) δ (ppm): -2.60 (br s, 2H, PdH₂), 0.35 (d, ³J_{H-H} = 6.4 Hz, 6H, CHMe₂), 0.76 – 2.21 (series of overlapping m, CHMe₂, Me, PCy₃), 2.87 (sept, ³J_{H-H} = 6.4 Hz, 2H, CHMe₂), 3.27 (sept, ³J_{H-H} = 6.8 Hz, 2H, CHMe₂), 3.44 (sept, ³J_{H-H} = 6.8 Hz, 2H, CHMe₂), 3.49 (sept, ³J_{H-H} = 6.4 Hz, 2H, CHMe₂), 4.85 (s, 2H, β-CH), 6.95-7.20 (series of overlapping m, Ar). ³¹P-{¹H}-NMR (202 MHz, C₆H₆) δ (ppm): 37.08 (s). **T₁ relaxation time** (PdH₂ signal, 298K): 0.60 s. **Crystal data for 2b**: C₇₆H₁₁₇Mg₂N₄PPd·C₆H₁₄, *M* = 1358.89, triclinic, *P*-1 (no. 2), *a* = 14.8889(15), *b* = 16.1336(10), *c* = 17.0165(11) Å, α = 96.422(5), β = 97.216(7), γ = 97.942(7)°, *V* = 3981.4(6) Å³, *Z* = 2, *D_c* = 1.134 g cm⁻³, μ(Cu-Kα) = 2.534 mm⁻¹, *T* = 173 K, pale yellow plates, Agilent Xcalibur PX Ultra A diffractometer; 15070 independent measured reflections (*R*_{int} = 0.0850), *F*² refinement, *R*₁(obs) = 0.0685, *wR*₂(all) = 0.1857, 10575 independent observed absorption-corrected reflections [|*F*_o| > 4σ(|*F*_o|)], 2θ_{max} = 148°, 833 parameters. CCDC 1589323. **Solution stability:** **2b** forms a complex equilibrium mixture in solution with not only [Pd(PCy₃)₂] and [Mg(μ-H){(ArNCMe)₂CH}]₂ but also **1a** in hydrocarbon solutions at 25 °C.

Synthesis of 2c: In a glovebox, [Mg(μ-H){(ArNCMe)₂CH}]₂ (58.4 mg, 0.066 mmol, 1.0 equiv.) and [Pt(PCy₃)₂] (50 mg, 0.066 mmols, 1.0 equiv.) were dissolved in dry benzene (3 mL) in a small ampoule. The resulting yellow solution was stirred at 25 °C for 3 h. The solvent was then removed *in vacuo*. The crude was dissolved in a small amount of dry *n*-hexane (0.5 mL), the excess [Mg(μ-H){(ArNCMe)₂CH}]₂ was removed by filtration through a glass fibre and the yellow clear solution was stored at -35 °C to afford the desired product **2c** as a pale yellow microcrystalline solid (85 mg, 0.062 mmol, 95 %). ¹H-NMR (500 MHz, C₆D₆, 298 K) δ (ppm): -6.25 (d, ²J_{H-Pt} = 8.5 Hz and ¹J_{H-Pt} = 833 Hz – satellites, 2H, PtH₂), 0.48 (br s, 3H), 1.03 – 1.95 (series of overlapping m, CHMe₂, Me, PCy₃), 2.77 (br sept, ³J_{H-H} = 6.4 Hz, 2H, CHMe₂), 3.39 (br sept, ³J_{H-H} = 6.8 Hz, 2H, CHMe₂), 3.47 (br sept, ³J_{H-H} = 6.8 Hz, 2H, CHMe₂), 3.56 (br sept, ³J_{H-H} = 6.4 Hz, 2H, CHMe₂), 4.92 (s, 2H, β-CH), 6.91-7.30 (series of overlapping m, Ar). **T₁ relaxation**

time (PtH₂ signal, 298K): 0.87 s. ³¹P-¹H-NMR (202 MHz, C₆H₆) δ (ppm): 44.04 (s, ¹J_{P-Pt} = 1600 Hz – satellites). ¹⁹⁵Pt-¹H-NMR (107.5 Hz, C₆H₆) δ (ppm): -5619.1 (d, ¹J_{P-Pt} = 1600 Hz). ¹³C-¹H-NMR (126 MHz, C₆H₆) δ (ppm): 23.7–29.2 (series of overlapping signals, CHMe₂, Me, PCy₃, CHMe₂), 30.8 (br s, 6xCH₂), 38.0 (d, ¹J_{C-P} = 12 Hz, 3xCH), 97.8 (2xCH), 123.2 (2xCH), 123.3 (2xCH), 124.0 (2xCH), 124.1 (2xCH), 125.3 (2xCH), 125.8 (2xCH), 142.2 (2xC), 142.4 (2xC), 143.1 (2xC), 144.0 (2xC), 146.3 (2xC), 147.0 (2xC), 168.3 (2xC), 168.7 (2xC). IR (ATR, cm⁻¹): 3058, 2957, 2924, 2850, 1661, 1622, 1550, 1524, 1460, 1435, 1408, 1382, 1362, 1314, 1254, 1174, 1100, 1020, 793, 759. Anal. Calc. (C₇₆H₁₁₇Mg₂N₄PtP): C, 67.05; H, 8.66; N, 4.12. Found: C, 66.40; H, 8.77; N, 3.86. **Crystal data for 2c:** C₇₆H₁₁₇Mg₂N₄PPt·1.35(C₆H₁₄), *M* = 1477.74, triclinic, *P*-1 (no. 2), *a* = 13.2111(3), *b* = 15.1411(4), *c* = 42.2615(12) Å, α = 83.607(2), β = 88.005(2), γ = 78.713(2)°, *V* = 8237.8(4) Å³, *Z* = 4 (2 molecules per asymmetric unit), *D*_c = 1.192 g cm⁻³, μ(Cu-Kα) = 3.828 mm⁻¹, *T* = 173 K, colourless needles, Agilent Xcalibur PX Ultra A diffractometer; 31579 independent measured reflections (*R*_{int} = 0.0426), *F*² refinement, *R*₁(obs) = 0.0407, *wR*₂(all) = 0.0977, 23332 independent observed absorption-corrected reflections [|*F*_o| > 4σ(|*F*_o|)], 2θ_{max} = 148°, 1630 parameters. CCDC 1909689.

Synthesis of 3: In a glovebox, [{(MesNCMe)₂CH}Mg]₂ (Mes = 2,4,6-trimethylphenyl, 100 mg, 0.14 mmol, 4.0 equiv.) and [Ni(PCy₃)₂]₂(μ-N₂) (44 mg, 0.03523 mmol, 1 equiv.) were transferred to a Young's tap ampoule. Benzene (5 mL) was added and the reaction was heated at 80 °C for 16 h. The reaction mixture was allowed to cool to 25 °C and *n*-hexane (5 mL) was added. Yellow crystals of **3** formed after standing overnight at 25 °C. The crystals were isolated by filtration and washed with *n*-hexane to give **3** as a yellow solid (93 mg, 0.066 mmol, 95 % yield). ¹H NMR (400 MHz, THF-*d*₈, 273 K): -7.27 (s, 3H, Mg-H-Ni), 0.06 (m, 3H), 0.42 (m, 3H), 0.52 (m, 3H), 0.75-0.94 (m, 12H), 1.01 (m, 3H), 1.36 (s, 9H), 1.41 (s, 9H), 1.54 (s, 9H), 1.54 (s, 9H), 1.57 (m, 6H), 1.95 (s, 9H), 2.07 (s, 9H), 2.10 (s, 9H), 2.23 (s, 9H), 2.46 (s, 9H), 5.09 (s, 3H), 6.60 (s, 3H), 6.65 (s, 3H), 6.80 (s, 3H), 7.07 (s, 3H). ³¹P{¹H} NMR (162 MHz, THF-*d*₈, 273 K): 53.6 ppm (s, PCy₃). ¹³C{¹H} NMR (100 MHz, THF-*d*₈, 273 K): 19.6 (CH₃), 19.8 (CH₃), 20.3 (CH₃), 20.7 (CH₃), 21.2 (CH₃), 22.0 (CH₃), 23.5 (CH₃), 24.4 (CH₃), 27.6, 28.1, 28.2, 28.5, 28.6, 30.2, 31.3, 31.4, 32.5, 35.1, 35.2, 98.0, 128.8 (C), 128.9 (CH), 130.2 (CH), 130.2 (CH), 130.8 (CH), 131.7 (C), 132.6 (C), 132.8 (C), 132.9 (C), 133.4 (C), 147.2 (C), 148.4 (C), 168.2 (C), 168.3 (C). Anal. Calc. (C₈₇H₁₂₃Mg₃N₆NiP): C, 73.82; H, 8.76; N, 5.94. Found: C, 73.67; H, 8.82; N, 5.59. **Crystal**

data for 3: X-ray: $C_{87}H_{123}Mg_3N_6NiP \cdot 3(C_6H_6)$, $M = 1649.84$, triclinic, $P-1$ (no. 2), $a = 14.2326(5)$, $b = 14.4809(4)$, $c = 24.0822(9)$ Å, $\alpha = 78.865(3)$, $\beta = 79.981(3)$, $\gamma = 84.955(2)^\circ$, $V = 4788.0(3)$ Å³, $Z = 2$, $D_c = 1.144$ g cm⁻³, $\mu(\text{Cu-K}\alpha) = 1.004$ mm⁻¹, $T = 173$ K, yellow blocks, Agilent Xcalibur PX Ultra A diffractometer; 18329 independent measured reflections ($R_{\text{int}} = 0.0393$), F^2 refinement, $R_1(\text{obs}) = 0.0439$, $wR_2(\text{all}) = 0.1154$, 13714 independent observed absorption-corrected reflections [$|F_o| > 4\sigma(|F_o|)$], $2\theta_{\text{max}} = 148^\circ$], 1084 parameters. CCDC 1909690.

Neutron data for 3: See SI for full details: Neutron Laue data were collected on the KOALA instrument at ANSTO. A total of 102728 reflections with wavelengths between 0.85 and 1.70 Å covering the full sphere of reciprocal space to a maximum resolution of 0.98 Å were reduced to yield 8847 independent reflections [$L4R(\text{int}) = 0.10(7)$]; 4816 with $I > 3\sigma(I)$. Refinement of a structure model in CRYSTALS converged to $R_1 = 0.1117$, $wR_2 = 0.0985$ for $I > 3\sigma(I)$. Max. and min. residual difference densities: 1.16 and -1.50 fermi Å⁻³.

Author Contributions

MG and CB carried out the synthetic studies. MG conducted DFT, QTAIM and related calculations. AJPW collected, processed and refined single-crystal X-ray diffraction data. AJE, RIC and GAS undertook the single-crystal Laue neutron diffraction experiment, data reduction and refined the neutron diffraction structural model. MRC managed the project. All authors contributed to the writing and editing of the manuscript.

Competing Interests

The authors declare no competing interests.

Data Availability Statement.

Crystallographic models are available as .cif files are available from from the Cambridge Crystallographic Data Centre (CCDC 1589323–1589324, 1909687–1909690). X-ray data Neutron diffraction images can be obtained from AJE. The derived structure factors have been deposited with the CCDC 1946045. Data associated with DFT calculations (.xyz coordinate file) along with NMR spectroscopic data (.mnova files) are available from a public repository: DOI: 10.14469/hpc/5985 (access code 3rrh-2k93). Full details of the syntheses are provided in the supplementary information.

Extended Data Legends

